Conjugated Polycycles

Deutsche Ausgabe: DOI: 10.1002/ange.201601517
Internationale Ausgabe: DOI: 10.1002/anie.201601517

Structural Polymorphism and Thin Film Transistor Behavior in the Fullerene Framework Molecule 5,6;11,12-di-*o*-Phenylenetetracene

*Tobias Wombacher, Andrea Gassmann, Sabine Foro, Heinz von Seggern, and Jörg J. Schneider**

Abstract: *The molecular structure of the hydrocarbon 5,6;11,12-di-o-phenylenetetracene (DOPT), its material characterization and evaluation of electronic properties is reported for the first time. A single-crystal X-ray study reveals two different motifs of intramolecular overlap with herringbone-type arrangement displaying either face-to-edge or co-facial face-to-face packing depicting intensive π–π interactions. Density functional theory (DFT) calculations underpin that a favorable electronic transport mechanism occurs by a charge hopping process due to a π-bond overlap in the DOPT polymorph with co-facial arene orientation. The performance of polycrystalline DOPT films as active organic semiconducting layer in a state-of-the-art organic field effect transistor (OFET) device was evaluated and proves to be film thickness dependent. For 40 nm layer thickness it displays a saturation hole mobility (μ_{hole}) of up to 0.01 $cm^2 V^{-1} s^{-1}$ and an on/off-ratio (I_{on}/I_{off}) of 1.5×10^3.*

The carbon framework in the title molecule is found as a basic structural motif in the fullerene molecules C_{78}, C_{82} and C_{84} (Figure 1). In addition, other symmetrical geodesic fullerene isomers bearing isolated pentagonal ring structures display molecular units of this conjugated polycycle.

5,6;11,12-di-*o*-phenylenetetracene (DOPT; **2**) belongs to the class of tetracene derivatives which have spurred interest over the last decade as model compounds with respect to an understanding of their chemistry as well as of their electronic properties like electronic structure and charge transport ability.[1,2] In the group of cyclo-pentafused polycyclic aromatic hydrocarbons (PAH) **2** represents a prototypical acene framework molecule with peri-substitution closely related to tetracene, 5,6,11,12-tetraphenyltetracenerubrene, or the di-*o*-phenylene substituted anthracene molecule rubicene.[2]

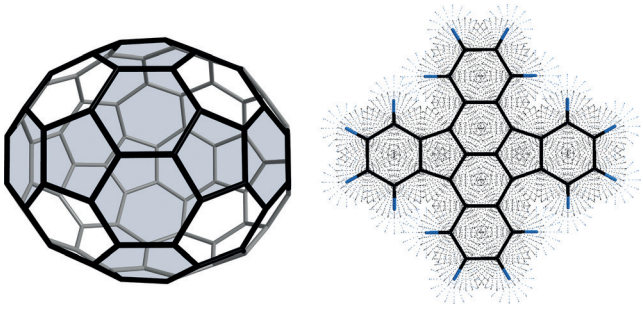

Figure 1. Left: Superordinated structure of 5,6;11,12-di-*o*-phenylenetetracene (DOPT, **2**) as found in e.g., the D_{2d} isomer of the geodesic fullerene C84. Right: Illustration of the all-planar cruciform structure of DOPT.

Although, reported earlier in elusive experimental work[3] it was only very recently, that DOPT **2** was made accessible by Murata[4] and our group[5] in two independent and straightforward high yield synthetic approaches. Murata et al. presented a general approach towards cyclo-pentafused polycyclic aromatics including DOPT-derivatives starting from the 5,11-diaryl-tetracene framework.[4] Shortly after, we were able to devise a gram-scale synthesis based on well established Diels–Alder chemistry for the parent molecule DOPT introducing a so far unprecedented reductive double phenyl elimination.[5] Highly condensed PAH molecules like DOPT with their oftentimes energetically favorable molecular orbital ordering with small electronic band gap differences excel themselves as promising semiconducting organic materials for controlled charge transport. The afore mentioned close structural relationship of DOPT to the polyacene aromatic family especially the parent tetracene might promise interesting functional properties applicable in organic electronics like thin film transistors or future solar energy harvesting devices.[6]

From a synthetic point of view the acene molecule DOPT is highly stable under ambient conditions when compared to other substituted tetracene derivatives. This is understandable when applying the Clar aromatic sextet model which states that a molecule with more benzenoid sextet moieties increases its aromatic stabilization energy.[7] Moreover the fact that DOPT **2** is able to accept at least up to two electrons[4,5] manifests its high electron affinity and makes it potentially suited for organic semiconductor applications. In this regard it falls into the same class of electroactive molecules as indenofluorenes, emaraldicenes or (silylethynylated) extended π-systems which have been proven as electron accepting as well as ambipolar molecules in organic

[*] Dipl.-Ing. T. Wombacher, Prof. Dr. J. J. Schneider
Eduard-Zintl-Institut für Anorganische und Physikalische Chemie, Technische Universität Darmstadt
Alarich-Weiss-Strasse 12, 64287 Darmstadt (Germany)
E-mail: joerg.schneider@ac.chemie.tu-darmstadt.de
Dr. A. Gassmann, Prof. H. von Seggern
Institut für Material- und Geowissenschaften, Technische Universität Darmstadt, Fachgebiet Elektronische Materialeigenschaften
Alarich-Weiss-Strasse 2, 64287 Darmstadt (Germany)
S. Foro
Institut für Material- und Geowissenschaften, Technische Universität Darmstadt, Fachgebiet Strukturforschung (Germany)

Supporting information (thermogravimetric analysis-mass spectrometry (TG-MS) and cyclovoltammetric (CV) data of **2**, mass spectrometric (MS) data of **2** recovered from the as-fabricated OFET units, XPS spectra of 5, 10, 20 and 40 nm films of **2** on SiO_2, and crystal structure parameters of both polymorphs of **2**) and the ORCID identification number(s) for the author(s) of this article can be found under http://dx.doi.org/10.1002/anie.201601517.

photovoltaics and organic field effect transistor applications.[1a,8] Furthermore, such large size PAH molecules have the capability of coordinating transition metals onto their π-perimeter framework giving access to organometallics acting as electroactive molecules which can carry up to four molecules of redox active metal fragments.[9] Additionally, such extended π-perimeters show a remarkably high electron affinity when exposed to strong reductive conditions, in turn leading to highly charged polyanions accompanied by a change in the structural shape of the particular neutral PAH.[10] Herein we report on the single crystal structure and thin film crystal orientation and phase formation of the title compound **2** as well as on its electronic properties as studied by experiment and density functional calculations (DFT). Finally, we give evidence towards the dependence of its electronic thin film transistor properties on the deposited film density. According to our finding, reductive elimination of two phenyl rings from the dihydrotetracene derivative 5,12-diphenyl-5,6;11,12-di-*o*-phenylene-5,12-dihydrotetracene(p-seudorubrene) **1** under re-aromatization has yielded DOPT **2** in high yield on a gram scale.[5]

As an extension of these studies we now report on the molecular structure of **2**. We have found that it crystallizes at least in two polymorphic crystal arrangements depending on the crystallization procedures employed. Growth from a concentrated tetrahydrofuran or toluene solution gives single crystals of DOPT which crystallize in space group *C* 2/*c*, whereas slow thermal gradient sublimation gives deep blue, primitive monoclinic crystals of space group *P* $2_1/n$ (see Supporting Information).

Thus, we speculated that the observed difference in the molecular arrangement of DOPT in the crystalline state might enable different charge-transport properties. As reported e.g., for tetracene,[11–13] rubrene,[13] rubicene[8f,14] or pentacene,[11b,15a,16] **2** adopts the well established herringbone-type structure orientation of individual molecules in the crystalline state (Figure 2). However, significant differences within the particular degree of the observed π-stacking are found in both polymorphs of **2**. Both monoclinic polymorphs of **2** consist of two sets of parallel aligned layers of DOPT molecules with different dihedral angles between two DOPT molecules (*P* $2_1/n$ polymorph: 84°; polymorph *C* 2/*c*: 64°). The π-framework of individual molecules of **2** is almost flat and displays a double cross-conjugation of the acene and the peri-condensed phenylene moieties as derived from the observed C–C bond-length alternation (Figure 2a). The observed intramolecular overlap between adjacent molecules of DOPT within the parallel stacked layer enables an electronic interplay of the HOMO–LUMO π-orbitals by [π–π]- and [C–H·π]-interactions necessary for an efficient charge transport within the stack.[2,15]

For the *P* $2_1/n$ phase of **2** the distance $d(\pi\text{–}\pi)_{core}$ between two staggered molecules of $DOPT_A$ and $DOPT_B$ is smallest for $C8_A$–$C2'_B$ with 345 pm which compares nicely to the interplanar distance of 338 pm between two adjacent molecules in rubicene crystals of space group *P* $2_1/n$.[14] The peri-coordinated phenylene units in **2** exhibit a closest distance $d(\pi\text{–}\pi)_{peri}$ to neighboring molecules by 368 pm for $C14_A$–$C11'_B$. In contrast, for the *C* 2/*c*-phase a nearly full π-overlap

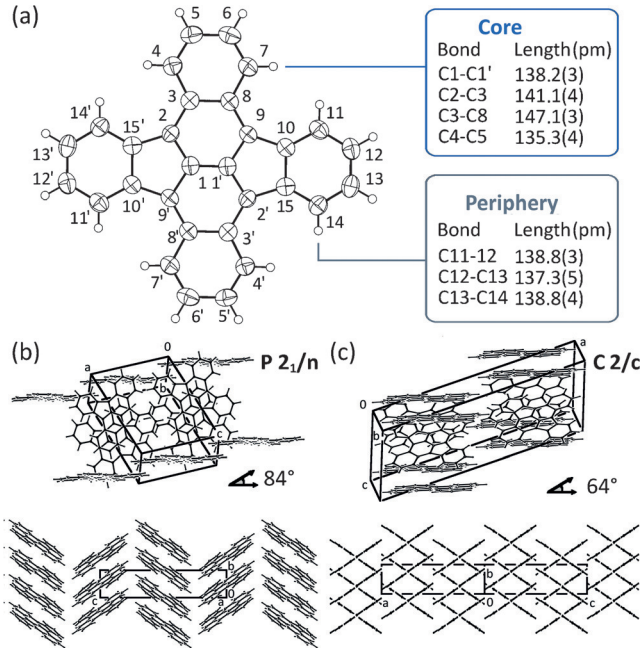

Figure 2. ORTEP plot of **2** with ellipsoids drawn at 50% probability level. The tetracenic backbone of **2** is fully planar. The plane of the two orthogonal phenylene rings deviate only by < 1° from planarity towards the plane of the tetracene ring system. Polymorph *P* $2_1/n$ (b) displays a herringbone structure with edge-to-face interactions of the DOPT molecules whereas polymorph *C* 2/*c* shows a co-facial herringbone arrangement with characteristic face-to-face π-interactions of neighboring DOPT molecules within the unit cell.

of the two staggered π-systems is observed, resulting in an overall denser packing of staggered DOPT layers in this polymorph (e.g. $\rho_{calcd}(P\ 2_1/n) = 1.387\ g\,cm^{-3} < \rho_{calcd}(C\ 2/c) = 1.412\ g\,cm^{-3}$) (Figure 3).

The tetracenic core and the peripheric phenylene rings of staggered **2** are in close contact displaying distances of 349 and 356 pm, respectively. These findings for **2** are in line with structural motifs found for reported polymorphs of the parent tetracene molecule,[12,13] the tetracene derivative rubrene[13,17] or for higher homologue pentacene[16] as well as other related structures.[8i]

As gas phase deposition of PAHs most often leads to a typical herringbone orientation with edge-to-face packing, it was surprising that indeed vacuum deposited films of **2** exclusively reveal the *C* 2/*c* polymorph when deposited on Si/SiO_2 substrate (see GIXRD, Figure 4). The *C* 2/*c* slipped π-stacking motive of **2** favors a better face-to-face overlap compared to the edge-to-face arrangement with its nearly orthogonal π–π stacked orientation of two DOPT molecules.

In contrast to the *P* $2_1/n$ phase obtained when **2** is sublimed onto a glass surface (calcd: 11.05, 16.24, 25.50° 2θ), the major reflections at 8.10/16.35° 2θ in GIXRD experiments give distinct evidence for the full staggered packing mode (calcd: 8.18, 16.40, 24.41° 2θ; exp: 8.08, 16.30° 2θ) of **2** in *C* 2/*c*. The preferred growth of the polymorphic orientation of **2** on Si/SiO_2 might be due to a substrate induced epitaxial re-orientation as found for rubicene and has been nicely shown by Winkler et al.[14] Crystalline **2** obtained from solution as well as from the gas phase indeed reveals strong anisotropic

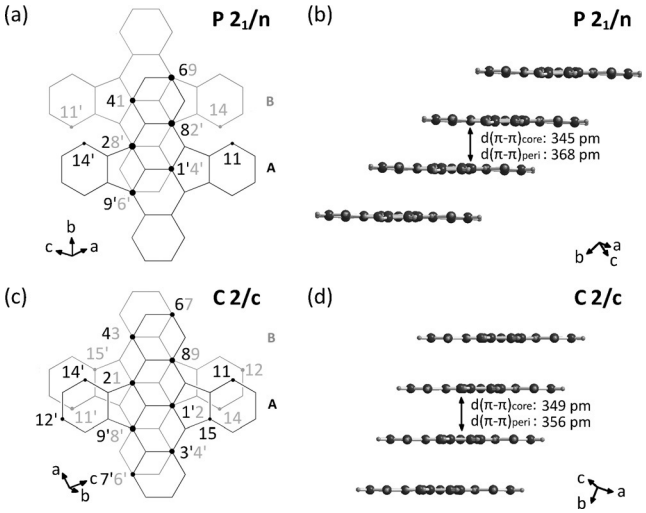

Figure 3. Illustration of the orientation and intermolecular distance between two individual molecules DOPT A and DOPT B in both monoclinic polymorphs. Dot size in (a) and (c) inversely corresponds to C–C distance of carbon atoms in adjacent DOPT molecules. The largest C_A–C_B distance is highlighted with the smallest dot. For the *P* $2_1/n$ polymorph (a), a displacement by two C–C bonds compared to the *C* 2/*c* type (b) is observed, resulting in a distinctively increased face-to-face π-stacking for the latter.

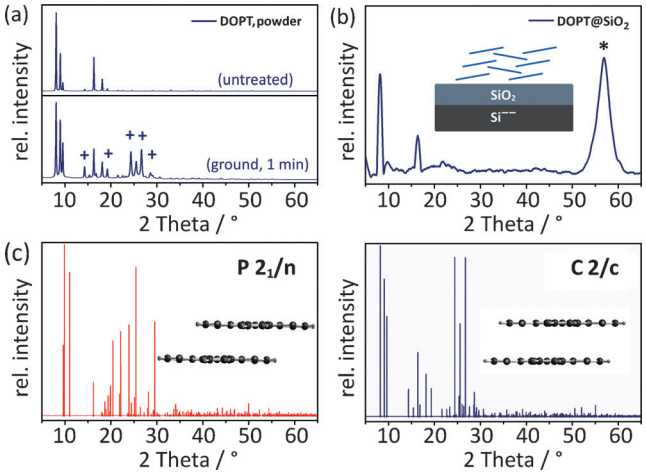

Figure 4. a) XRD pattern of microcrystalline DOPT **2** obtained from solution and after grinding; b) GIXRD pattern with a cartoon showing the face-to-face interaction of individual molecules in a thin film of vacuum deposited crystalline **2** on Si/SiO_2(*); c) calculated spectra showing all possible reflections (lower trace).

texturing effects resulting in significant diminution of higher order reflections for both polymorphs in XRD and GIXRD (Figure 4). This effect could be verified by strong mechanical grinding of a crystalline sample of **2.** This generates the missing higher order reflections due to a sample homogenization (see Supporting Information).

In order to understand the substrate influence better, the morphology of vacuum deposited DOPT films was evaluated for 5, 10, 20 and 40 nm layers of **2** by atomic force microscopy (AFM, Figure 5). All macroscopic homogeneously appearing films are composed of randomly distributed thin needles of up

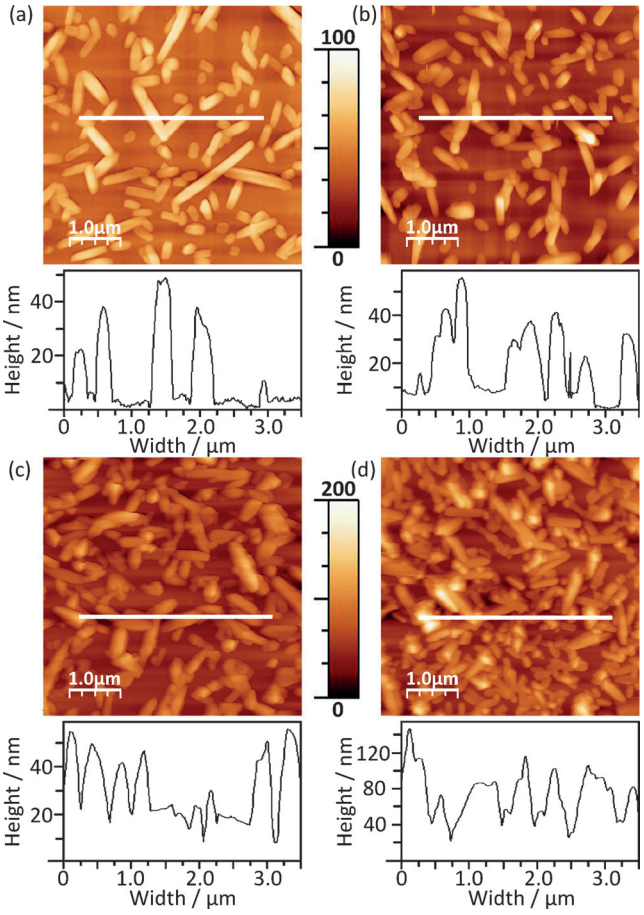

Figure 5. AFM topographic images obtained for film heights *h*: a) 5 nm, b) 10 nm, c) 20 nm, d) 40 nm of **2** (white bars indicate scan direction). All deposited films consist of randomly oriented thin needles of ca. 1 μm in length. With increasing DOPT layer thickness enhanced crystal overlap and compacted packing is observed.

to two microns in length. Depending on the deposition thickness the needle-like thin film thickness increases considerably (Figure 5 a–d). Due to the observed film morphology the growth mechanism of **2** is in full accordance with observations on film growth of closely related rubicene on Si/SiO_2 substrate.[14] Thus, mainly Ostwald ripening of the initially adsorbed molecules leads to an anisotropic island growth of crystals of **2** preventing the development of a homogeneous thin film. Furthermore, we analyzed all thin films of **2** by UV/Vis transmission mode in order to correlate the absorption spectra to the varying film thickness (5, 10, 20, and 40 nm) (Figure 6) and to validate evidence of the so far observed structural ordering what has also an effect on the electronic behavior.[18]

Compared to the UV/Vis spectra obtained from $CHCl_3$ solution, a J-aggregation[19] is observed and manifests itself by a strong bathochromic shift (+63 nm) to longer wavelength ($\lambda_{max\ (l)}$[5]/ $\lambda_{max\ (s),40\ nm}$: 607.5/670.5 nm).

DFT calculations on B3LYP/6-31G**[20] level give the frontier orbital energy of the participating HOMO/LUMO orbitals of DOPT and reveal a significantly enhanced orbital overlap for the face-to-face π-stacking mode of the *C* 2/*c* compared to the *P* $2_1/n$ polymorph (Figure 7). The exper-

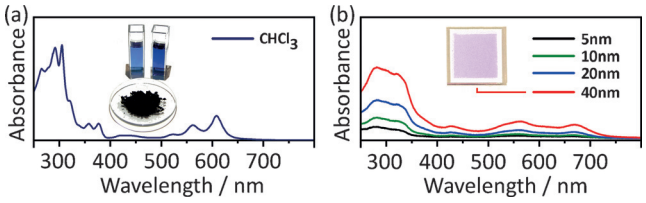

Figure 6. a) UV/Vis-spectra of **2** in $CHCl_3$ solution and b) in solid films of different thickness ($h = 5$, 10, 20, 40 nm). $E_{g,opt}$ is reduced from ≈1.86 eV in solution down to ≈1.70 eV in the solid state. A strong bathochromic shift (+63 nm) due to J-aggregation effects is observed for the absorption at longer wavelength (607.5→670.5 nm).[19]

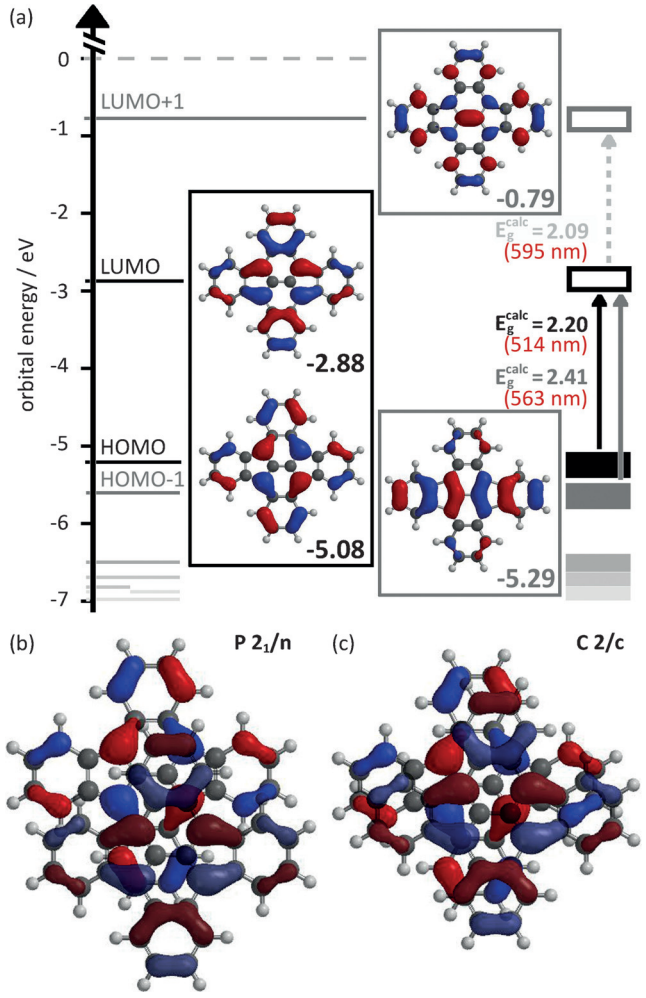

Figure 7. a) Predicted frontier orbitals HOMO−1, HOMO, LUMO and LUMO+1 of DOPT **2** as obtained by DFT calculations (B3LYP/6-31G**).[20] The respective HOMO/LUMO overlap in both polymorphs of **2** is shown in (b) and (c).

imentally obtained bond length alternation derived from the crystal structure determination (Figure 2a) fully agrees with the size and sign of the calculated HOMO/LUMO set based on the DFT method (Figure 7a). Furthermore, the as calculated gaps between HOMO−1/HOMO (514 nm/2.41 eV), HOMO/LUMO (563 nm/2.20 eV) (and LUMO/LUMO+1 (595 nm/2.09 eV)) match well the recorded long-wave π–π* transitions, respectively, of the corresponding UV/Vis spectra (Figure 6). Cyclic voltammetry (CV) of **2** reveals a quasi-reversible (0/−1) reduction at −1.22 V ($\Delta E_p = 80$ mV) and a reversible reduction (−1/−2) at $E^{red}_{1/2}$ −1.65 V ($\Delta E_p =$ 60 mV) which is in full agreement with our earlier proposed synthetic pathway leading to the formation of **2**.[5] Due to a lack of a reversible oxidation event $E^{ox}_{1/2}$ (0/+1) for **2** up to +1.0 V no direct determination of the corresponding band gap ΔE is possible. However, the LUMO energy of **2** is estimated to be −3.10 V (using $E^{red}_{0/-1} = -1.22$ V), respectively −2.67 V (using $E^{red}_{-1/-2} = -1.65$ V) according to the equation $E_{LUMO}(DOPT) = -[E^{red}(DOPT) - E^{ox}_{1/2}(Fc/Fc^+)] - E_{HOMO}(Fc)$[21] (see Supporting Information). Both values correspond well with the calculated energy of $E_{LUMO}(DOPT)$ of −2.88 eV (Figure 7a). The HOMO and LUMO frontier orbital interaction for both polymorphs corroborates the strongest positive overlap for the face-to-face π-stacking mode observed in *C* 2/*c* polymorph of **2** (Figure 7c) resulting in an apparently most complete interaction of the conjugated phenylene moieties.[2,15,22] Subsequently, vacuum deposited DOPT was studied as semiconductor for organic field-effect transistors employing a bottom-gate/bottom-contact geometry (Figure 8a). It is expected that the full planar structure of **2** is a most favorable precondition for a good crystallinity of the evaporated layer favoring in addition lateral π–π stacking at the semiconductor/dielectric interface. Due to its face-to-face structural motif found in the co-facial herringbone arrangement, the *C* 2/*c* polymorph of DOPT **2** is a promising candidate for OFET applications.[2]

Figure 8b shows the output and transfer curves that have been obtained for OFET devices fabricated using a 40 nm thick vacuum deposited DOPT layer. 16 OFET devices with 40, 20, 10 and 5 nm thick layers of **2** were evaluated, respectively, for four different channel lengths of 20, 10, 5, and 2.5 μm each (see Supporting Information). All output curves of the devices with 40 and 20 nm DOPT thickness exhibit a typical transistor like saturation behavior displaying a small current hysteresis. For low drain voltages a slight S-shape of the curve is evident for 40 nm DOPT layer pointing to injection barriers between the gold contacts and the organic semiconductor. This finding is in line with the results from the DFT calculations (Figure 7a) which yield a HOMO level of 5.08 eV. Assuming a work function of 5.1 eV for gold[23] a small injection barrier of 0.02 eV results. Prototypical transistor behavior with a current saturation in the output curves has been observed with only slight hysteresis with a 20 nm functional DOPT layer. The observed drain current is already about a factor of 10 smaller. Devices with 10 nm and 5 nm DOPT however, were not functional at all. This corroborates with the detection of a non-uniform coverage of the substrate as detected by AFM and does already become noticeable with 20 nm DOPT as active layer (Figure 5). Measurements with a drain voltage in the positive potential range from 0 V to +40 V did not show any n-type semiconducting behavior (see Supporting Information). Overview of the detailed analysis of the determined hole mobilities μ_{hole} and threshold voltages V_{th} of all functional devices are given in Figure 8c as function of the channel length *L*. Both quantities have been calculated from the transfer curves using the Shockley equations[24] for the drain current. The

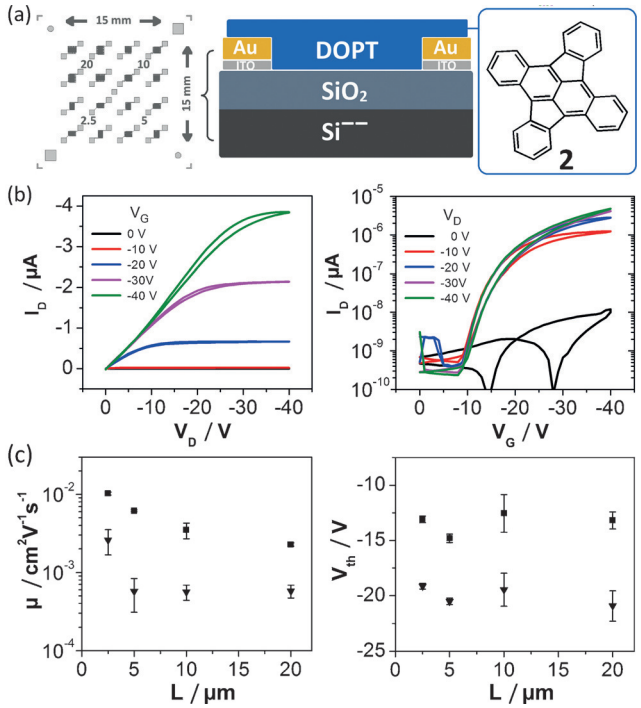

Figure 8. a) Illustration of OFET device structure in bottom-gate/bottom-contact geometry. A highly n-doped silicon gate (Si^{--}) with isolating top layer of SiO_2 (90 nm) and deposited Au (30 nm) electrodes was used as source and drain electrodes and 10 nm indium tin oxide electrode adhesion layer. b) Output (left) and logarithmic transfer curves (right) of transistor behavior with 40 nm layer of **2**. The *W*/*L* ratio is 1000, corresponding to a channel length *L* of 10 µm and a width *W* of 10 mm. The on/off-ratio is up to 1.5×10^3 (for $V_D = V_G = -40$ V). c) Average hole mobilities μ_{hole} (left) and threshold voltages (right) as a function of channel length for various transistor devices. The values illustrated with squares have been calculated for the devices with 40 nm semiconductor, the triangles relate to values from OFET devices with 20 nm thick functional layers of **2**.

calculated hole mobility of DOPT is in the range of 10^{-3} $cm^2V^{-1}s^{-1}$. However, apparent differences are observed for the transistors with 40 nm or 20 nm DOPT layer. It is evident that OFET devices with 40 nm DOPT layer exhibit considerably higher μ_{hole} up to 0.01 $cm^2V^{-1}s^{-1}$ (for $L =$ 2.5 µm) compared to the OFET devices with 20 nm DOPT which are up to 1.5×10^{-3} $cm^2V^{-1}s^{-1}$. The associated V_{th} of the devices prepared with 40 nm DOPT are rather independent on the channel length and lay around −13.4 V. This is significantly higher compared to V_{th} of the devices with 20 nm DOPT which are around −20.0 V. As V_{th} is directly related to the quality of the semiconductor/dielectric interface, for example, the interface trap density, these results indicate that the interface has a lower trap density in the case of OFET with 40 nm compared to the one with 20 nm thick DOPT layer. Although the DOPT molecules are well behaved with respect to their internal crystalline order (packing) of the molecules the crystallites are obviously not densely enough packed to allow for an optimal charge carrier transport along the transistor channel for a semiconductor thickness of 20 nm. This hypothesis is strongly substantiated by the AFM studies (Figure 5). The fact that μ_{hole} is found to be maximum for the respective shortest channels is supporting this, as longer channels increase the probability for defects, for example, voids, in the conduction path. One method to improve the crystal packing of a layer is its post heat treatment. Therefore, the as prepared OFET with a DOPT layer thickness of 40 nm have been additionally heat treated under inert conditions on a hot plate at 120 °C for 30 min. Indeed, μ_{hole} can be enhanced to some extent in this way. Compared to so far reported optimized OFET devices obtained from tetracene (vapor phase deposited: 0.005 $cm^2V^{-1}s^{-1}$; resp. solution processed: 0.012–0.067 $cm^2V^{-1}s^{-1}$)[1a] or pentacene (vapor phase deposited: 0.014–0.40 $cm^2V^{-1}s^{-1}$)[8n,u] as semiconductor layer, already similar charge carrier mobilities of 0.01 $cm^2V^{-1}s^{-1}$ could be realized for the title compound DOPT herein without optimizing the deposition parameters further.

In conclusion we have shown that the title compound **2** crystallizes in two molecular packing motifs depending on the crystallization deposition mode. Two polymorphs of DOPT crystallizing in space group *P* $2_1/n$ and *C* 2/*c* were observed and a strong substrate induced growth mechanism favoring the *C* 2/*c* phase in solution as well as on Si/SiO_2 was determined by GIXRD analysis. Based on theoretical considerations a strong intermolecular π–π stacking with a significant and stronger overlap contribution from the frontier orbitals was found for the DOPT molecules in the *C* 2/*c* phase as for the *P* $2_1/n$ polymorph. The intermolecular orientation and overlap contribution of participating HOMO/LUMO frontier orbitals in the *C* 2/*c* type gives strong evidence for an enhanced charge carrier transport mechanism in vacuum deposited DOPT. Gas phase deposition of **2** results in layers composed of needle-like aggregates and explains the strong dependence of the OFET performance characteristics from the deposited film thickness. In the end our findings give a profound explanation of the functional efficiency of the as prepared OFET devices of the relatively unexplored acene molecule **2**.

CCDC 1448430 and 1448442 contain the supplementary crystallographic data for this paper. These data can be obtained free of charge from The Cambridge Crystallographic Data Centre via www.ccdc.cam.ac.uk/data_request/cif.

Acknowledgements

Discussions as well as initial OFET measurements where done by S. Sanctis (TU Darmstadt) and are highly appreciated. Support by Dr. W. Brötz (GIXRD, TU Darmstadt) is acknowledged.

Keywords: fullerene · fused-ring systems · hydrocarbons · organic field effect transistor · polycycles

How to cite: *Angew. Chem. Int. Ed.* **2016**, *55*, 6041–6046
Angew. Chem. **2016**, *128*, 6145–6150

[1] a) C.-T. Chien, C.-C. Lin, M. Watanabe, Y.-D. Lin, T.-H. Chao, T. Chiang, X.-H. Huang, Y.-S. Wen, C.-H. Tu, C.-H. Sun et al., *J. Mater. Chem.* **2012**, *22*, 13070–13075; b) Y. Xia, V. Kalihari,

C. D. Frisbie, N. K. Oh, J. A. Rogers, *Appl. Phys. Lett.* **2007**, *90*, 162106 – 162108; c) R. Sarma, D. Saikia, *Indian J. Pure Appl. Phys.* **2009**, *47*, 876 – 879; d) C. R. Newman, R. J. Chesterfield, J. a. Merlo, C. D. Frisbie, *Appl. Phys. Lett.* **2004**, *85*, 422 – 425; e) Y. Yoon, S. Kim, H. Lee, T. Kim, A. Babajanyan, K. Lee, B. Friedman, *Thin Solid Films* **2011**, *519*, 5562 – 5566; f) H. M. Lee, H. Moon, H.-S. Kim, Y. N. Kim, S.-M. Choi, S. Yoo, S. O. Cho, *Org. Electron.* **2011**, *12*, 1446 – 1453; g) T. Hasegawa, J. Takeya, *Sci. Technol. Adv. Mater.* **2009**, *10*, 024314; h) V. Podzorov, V. M. Pudalov, M. E. Gershenson, *Appl. Phys. Lett.* **2003**, *82*, 1739 – 1741; i) V. Podzorov, S. E. Sysoev, E. Loginova, V. M. Pudalov, M. E. Gershenson, *Appl. Phys. Lett.* **2003**, *83*, 3504 – 3506.

[2] H. Dong, X. Fu, J. Liu, Z. Wang, W. Hu, *Adv. Mater.* **2013**, *25*, 6158 – 6183.

[3] a) C. Dufraisse, R. Buret, *C. R. Chim.* **1932**, *65*, 962 – 964; b) C. Dufraisse, R. Girard, *Mem. Soc. Chim.* **1934**, *5*, 1359 – 1367; c) C. Moureu, C. Dufraisse, C. Mackall, *Bull. Soc. Chim. Fr.* **1923**, *33*, 934 – 942; d) C. Dufraisse, R. Horclois, *Bull. Soc. Chim. Fr.* **1936**, *3*, 1894 – 1905; e) M. Badoche, *Ann. Chim.* **1933**, *20*, 200; f) K. F. Lang, E.-A. Theiling, *Chem. Ber.* **1956**, *89*, 2734 – 2737; g) G. Wittig, H. Härle, E. Knauss, K. Niethammer, *Chem. Ber.* **1960**, 951 – 962.

[4] Chaolumen, M. Murata, Y. Sugano, A. Wakamiya, Y. Murata, *Angew. Chem. Int. Ed.* **2015**, *54*, 9308 – 9312; *Angew. Chem.* **2015**, *127*, 9440 – 9444.

[5] T. Wombacher, S. Foro, J. J. Schneider, *Eur. J. Org. Chem.* **2016**, 569 – 578.

[6] G. Dai, J. Chang, W. Zhang, S. Bai, K.-W. Huang, J. Xu, C. Chi, *Chem. Commun.* **2015**, *51*, 503 – 506.

[7] E. Clar in *Polycyclic Hydrocarbons*, *Vol. I*, Academic Press, London, New York, Springer, Heidelberg, **1964**.

[8] a) D. T. Chase, B. D. Rose, S. P. McClintock, L. N. Zakharov, M. M. Haley, *Angew. Chem. Int. Ed.* **2011**, *50*, 1127 – 1130; *Angew. Chem.* **2011**, *123*, 1159 – 1162; b) D. T. Chase, A. G. Fix, B. D. Rose, C. D. Weber, S. Nobusue, C. E. Stockwell, L. N. Zakharov, M. C. Lonergan, M. M. Haley, *Angew. Chem. Int. Ed.* **2011**, *50*, 11103 – 11106; *Angew. Chem.* **2011**, *123*, 11299 – 11302; c) A. R. Mohebbi, F. Wudl, *Chemistry* **2011**, *17*, 2642 – 2646; d) A. R. Mohebbi, J. Yuen, J. Fan, C. Munoz, M. F. Wang, R. S. Shirazi, J. Seifter, F. Wudl, *Adv. Mater.* **2011**, *23*, 4644 – 4648; e) X. Gu, X. Xu, H. Li, Z. Liu, Q. Miao, *J. Am. Chem. Soc.* **2015**, *137*, 16203 – 16208; f) H. Lee, Y. Zhang, L. Zhang, T. Mirabito, E. K. Burnett, S. Trahan, A. R. Mohebbi, S. C. B. Mannsfeld, F. Wudl, A. L. Briseno, *J. Mater. Chem. C* **2014**, *2*, 3361 – 3366; g) L. Zhang, Y. Cao, N. S. Colella, Y. Liang, J.-L. Brédas, K. N. Houk, A. L. Briseno, *Acc. Chem. Res.* **2015**, *48*, 500 – 509; h) L. Zhang, A. Fonari, Y. Liu, A. M. Hoyt, H. Lee, D. Granger, S. Parkin, T. P. Russell, J. E. Anthony, J.-L. Brédas et al., *J. Am. Chem. Soc.* **2014**, *136*, 9248 – 9251; i) X. Yang, D. Liu, Q. Miao, *Angew. Chem. Int. Ed.* **2014**, *53*, 6786 – 6790; *Angew. Chem.* **2014**, *126*, 6904 – 6908; j) K. B. Burke, Y. Shu, P. Kemppinen, B. Singh, M. Bown, I. I. Liaw, R. M. Williamson, L. Thomsen, P. Dastoor, W. Belcher et al., *Cryst. Growth Des.* **2012**, *12*, 725 – 731; k) W. H. Lee, D. H. Kim, Y. Jang, J. H. Cho, M. Hwang, Y. D. Park, Y. H. Kim, J. I. Han, K. Cho, *Appl. Phys. Lett.* **2007**, *90*, 132106; l) M. R. Rao, H. T. Black, D. F. Perepichka, *Org. Lett.* **2015**, *17*, 4224 – 4227; m) T. Kawase, J.-I. Nishida, *Chem. Rec.* **2015**, *15*, 1045 – 1059; n) R. Scholz, A.-D. Müller, F. Müller, I. Thurzo, B. A. Paez, L. Mancera, D. R. T. Zahn, C. Pannemann, U. Hilleringmann in *Proc. SPIE 5940*, *Org. Field-Effect Transistors IV* (Eds.: Z. Bao, D. J. Gundlach), **2005**, 59400I-1 – 59400I-7; o) A. Bayn, X. Feng, K. Müllen, H. Haick, *ACS Appl. Mater. Interfaces* **2013**, *5*, 3431 – 3440; p) M. Bendikov, F. Wudl, *Chem. Rev.* **2004**, *104*, 4891 – 4946; q) Z. Sun, Q. Ye, C. Chi, J. Wu, *Chem. Soc. Rev.* **2012**, *41*, 7857 – 7889; r) D. T. Chase, A. G. Fix, S. J. Kang, B. D. Rose, C. D. Weber, Y. Zhong, L. N. Zakharov, M. C. Lonergan, C. Nuckolls, M. M. Haley, *J. Am. Chem. Soc.* **2012**, *134*, 10349 – 10352; s) H. Xia, D. Liu, X. Xu, Q. Miao, *Chem. Commun.* **2013**, *49*, 4301 – 4303; t) J. L. Jellison, C.-H. Lee, X. Zhu, J. D. Wood, K. N. Plunkett, *Angew. Chem. Int. Ed.* **2012**, *51*, 12321 – 12324; *Angew. Chem.* **2012**, *124*, 12487 – 12490; u) D. Knipp, R. A. Street, A. Völkel, J. Ho, *J. Appl. Phys.* **2003**, *93*, 347 – 355.

[9] a) J. J. Schneider, D. Spickermann, C. W. Lehmann, J. Magull, H.-J. Krüger, J. Ensling, P. Gütlich, *Chem. Eur. J.* **2006**, *12*, 1427 – 1435; b) J. J. Schneider, D. Spickermann, T. Labahn, M. Fontani, F. Laschi, P. Zanello, *Chem. Eur. J.* **2000**, *6*, 3686 – 3691; c) J. J. Schneider, D. Wolf, C. W. Lehmann, *Inorg. Chim. Acta* **2003**, *350*, 625 – 632; d) C. Elschenbroich, R. Mockel, A. Vasil′kov, B. Metz, K. Harms, *Eur. J. Inorg. Chem.* **1998**, *10*, 1391 – 1401; e) J. J. Schneider, D. Spickermann, D. Bläser, R. Boese, P. Rademacher, T. Labahn, J. Magull, C. Janiak, N. Seidel, K. Jacob, *Eur. J. Inorg. Chem.* **2001**, 1371 – 1382.

[10] a) A. V. Zabula, N. J. Sumner, A. S. Filatov, S. N. Spisak, V. M. Grigoryants, M. A. Petrukhina, *Eur. J. Inorg. Chem.* **2012**, 4675 – 4683; b) A. S. Filatov, N. J. Sumner, S. N. Spisak, A. V. Zabula, A. Y. Rogachev, M. A. Petrukhina, *Chem. Eur. J.* **2012**, *18*, 15753 – 15760; c) A. V. Zabula, A. S. Filatov, S. N. Spisak, A. Y. Rogachev, M. A. Petrukhina, *Science* **2011**, *333*, 1008 – 1011; d) A. V. Zabula, S. N. Spisak, A. S. Filatov, M. A. Petrukhina, *Angew. Chem. Int. Ed.* **2012**, *51*, 12194 – 12198; *Angew. Chem.* **2012**, *124*, 12360 – 12364; e) H. Bock, *Nachr. Chem.* **2001**, *49*, 18 – 21; f) C. Näther, H. Bock, Z. Havlas, T. Hauck, *Organometallics* **1998**, *17*, 4707 – 4715.

[11] a) E. Venuti, R. G. Della Valle, L. Farina, A. Brillante, M. Masino, A. Girlando, *Phys. Rev. B* **2004**, *70*, 104106; b) M. Brinkmann, S. Graff, C. Straupe, J. Wittmann, I. C. Sadron, C. Chaumont, F. Nuesch, A. Aziz, M. Schaer, L. Zuppiroli, *J. Phys. Chem. B* **2003**, *107*, 10531 – 10539.

[12] D. H. Arias, J. L. Ryerson, J. D. Cook, N. H. Damrauer, J. C. Johnson, *Chem. Sci.* **2016**, 41 – 44.

[13] S. Bergantin, M. Moret, *Cryst. Growth Des.* **2012**, *12*, 6035 – 6041.

[14] B. Scherwitzl, W. Lukesch, A. Hirzer, J. Albering, G. Leising, R. Resel, A. Winkler, *J. Phys. Chem. C* **2013**, *117*, 4115 – 4123.

[15] a) V. Coropceanu, J. Cornil, A. Demetrio, S. Filho, Y. Olivier, R. Silbey, J. Bre, *Chem. Rev.* **2007**, *107*, 926 – 952; b) C. R. Martinez, B. L. Iverson, *Chem. Sci.* **2012**, *3*, 2191 – 2201.

[16] a) C. C. Mattheus, G. A. De Wijs, R. A. De Groot, T. T. M. Palstra, *J. Am. Chem. Soc.* **2003**, *125*, 6323 – 6330; b) S. Schiefer, M. Huth, A. Dobrinevski, B. Nickel, *J. Am. Chem. Soc.* **2007**, *129*, 10316 – 10317.

[17] a) S. Uttiya, L. Miozzo, E. M. Fumagalli, S. Bergantin, R. Ruffo, M. Parravicini, A. Papagni, M. Moret, A. Sassella, *J. Mater. Chem. C* **2014**, *2*, 4147 – 4155; b) L. Huang, Q. Liao, Q. Shi, H. Fu, J. Ma, J. Yao, *J. Mater. Chem.* **2010**, *20*, 159 – 166.

[18] S. Venkatesan, E. C. Ngo, Q. Chen, A. Dubey, L. Mohammad, N. Adhikari, A. F. Mitul, Q. Qiao, *Nanoscale* **2014**, *6*, 7093 – 7100.

[19] F. Würthner, T. E. Kaiser, C. R. Saha-Möller, *Angew. Chem. Int. Ed.* **2011**, *50*, 3376 – 3410; *Angew. Chem.* **2011**, *123*, 3436 – 3473.

[20] The three parameter hybrid nonlocal exchange functional of Becke combined with the Lee–Yang–Parr gradient-corrected correlation functional was used (B3LYP), a) A. Becke, *J. Chem. Phys.* **1993**, *98*, 5648 – 5652; b) C. Lee, W. Yang, R. G. Parr, *Phys. Rev. B* **1988**, *37*, 785 – 789.

[21] M. M. Ahmida, S. H. Eichhorn, *ECS Trans.* **2010**, *25*, 1 – 10.

[22] L. Wang, G. Nan, X. Yang, Q. Peng, Q. Li, Z. Shuai, *Chem. Soc. Rev.* **2010**, *39*, 423 – 434.

[23] T. Yasuda, T. Goto, K. Fujita, T. Tsutsui, *Appl. Phys. Lett.* **2004**, *85*, 2098 – 2100.

[24] W. Shockley, W. T. Read, *Phys. Rev.* **1952**, *87*, 835 – 842.

Received: February 12, 2016
Revised: March 10, 2016
Published online: April 8, 2016

